Vol.2021-QS-3 No.3
2021/7/1

ハイブリッドテンソルネットワークにおける遷移振幅計算のための量子アルゴリズム

菅野 志優[1,a)]　遠藤 傑[2,b)]　鈴木 泰成[2,3]　徳永 裕己[2]

概要：The hybrid tensor network approach allows us to perform calculations on systems larger than the scale of a quantum computer. However, when calculating transition amplitudes, there is a problem that the number of terms to be measured increases exponentially with that of contracted operators. The problem is caused by the fact that the contracted operators are represented as non-Hermitian operators. In this study, we propose a method for the hybrid tensor network calculation that contracts non-Hermitian operators without the exponential increase of the number of terms. In the proposed method, calculations of transition amplitudes are performed by combining the singular value decomposition of the contracted non-Hermitian operators with the Hadamard test. The method significantly extends the applicability of the hybrid tensor network approach.

Quantum algorithm for calculation of transition amplitudes in hybrid tensor networks

1. Introduction

Quantum computers are expected to be capable of executing classically intractable calculations [1–7]. It has been reported that quantum computers can outperform classical computers in some tasks [8, 9]. However, quantum resource limitations become obstacles for practical applications to quantum computers. Current quantum computers are so-called noisy intermediate-scale quantum (NISQ) devices [10], and we can control only tens to hundreds of noisy qubits on the devices [4, 11–16]. The hardware limitations make it difficult to apply quantum computers to practical tasks that require large numbers of qubits or deep quantum circuits [17–29].

The hybrid tensor network approach has been proposed recently to overcome the obstacles for the limitations [17]. The approach enables the treatment of quantum states larger than actual quantum devices by representing quantum states with a combination of conventional classical tensors and quantum tensors. A quantum tensor has upper and lower indices as, for example, $\psi^{j_1,j_2\dots j_L}_{i_1,i_2\dots i_K}$, which represents K-qubit systems indexed by L-bit string. In other words, the quantum state is defined for L classical bits $(j_1, j_2, \dots, j_L)$ as

$$|\psi^{j_1,j_2,\dots j_L}\rangle = \sum_{i_1,i_2,\dots,i_K} \psi^{j_1,j_2,\dots,j_L}_{i_1,i_2,\dots,i_K} |i_1 i_2 \dots i_K\rangle\,, \quad (1)$$

where $\psi^{j_1,j_2,\dots,j_L}_{i_1,i_2,\dots,i_K} \in \mathbb{C}$, $\sum_{i_1,i_2,\dots,i_K} |\psi^{j_1,j_2,\dots,j_L}_{i_1,i_2,\dots,i_K}|^2 = 1$, and $|i_1 i_2 \dots i_K\rangle$ is a computational basis of the K-qubit Hilbert space. One of the most vital forms of the hybrid tensor network is a hybrid tree-tensor network, where a network of quantum and classical tensors constructs a tree graph. While the contraction of general hybrid tensor networks can be costly, hybrid tree-tensor networks can be contracted efficiently to obtain expectation values [17]. In this paper, we mainly discuss a two-layer hybrid tree-tensor network only with quantum tensors, which is called

[1] 東京工業大学 物質理工学院
Department of Materials Science and Engineering, Tokyo Institute of Technology
[2] NTT セキュアプラットフォーム研究所
NTT Secure Platform Laboratories, NTT Corporation
[3] JST さきがけ
JST, PRESTO
[a)] kanno.s.ac@m.titech.ac.jp
[b)] suguru.endou.uc@hco.ntt.co.jp

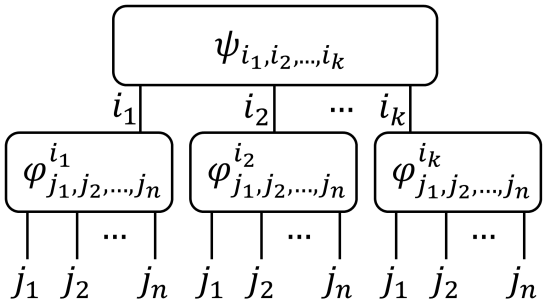

図 1 A quantum-quantum tree-tensor network as in Eq. (2). $\varphi^{i_m}_{j_1,j_2,\ldots,j_n}$ is defined as $\langle j_1 j_2 \ldots j_n|\varphi^{i_m}\rangle$. In quantum-classical tree-tensor network, $\psi_{i_1,i_2,\ldots,i_k}$ is replaced with a classical tensor, while in a classical-quantum tree-tensor network, classical tensors are used in place of $\varphi^{i_m}_{j_1,j_2,\ldots,j_n}$.

a quantum-quantum tree-tensor network, since it captures the essential properties of hybrid tree-tensor networks and the use of classical tensors restricts the range of representation to classically tractable quantum states such as matrix product states [30]. A quantum-quantum tree-tensor network that expresses k subsystems of n-qubit states is represented as

$$|\psi_{HT}\rangle = \sum_{i_1,i_2,\ldots,i_k} \psi_{i_1,i_2,\ldots,i_k} |\varphi^{i_1}\rangle \otimes |\varphi^{i_2}\rangle \otimes \cdots \otimes |\varphi^{i_k}\rangle, \tag{2}$$

where $|\psi_{HT}\rangle$ is unnormalized state, $\psi_{i_1,i_2,\ldots,i_k} = \langle i_1 i_2 \ldots i_k|\psi\rangle$ is a probability amplitude of a k-qubit state $|\psi\rangle$, and $|\varphi^{i_m}\rangle (m = 1, 2, \ldots, k)$ is an n-qubit state of the m-th subsystem indexed by a classical bit i_m. Figure 1 shows the network diagram of $|\psi_{HT}\rangle$. While the state $|\psi_{HT}\rangle$ represents a kn-qubit state, we can efficiently calculate the expectation value of an observable $O = \bigotimes_{m=1}^{k} O_m$, where O_m operates on $|\varphi^{i_m}\rangle$ via proper tensor contractions, using a quantum computer with $O(\max(k, n))$ qubits. The contraction for evaluating the expectation value $\langle O\rangle = \langle\psi_{HT}| O |\psi_{HT}\rangle$ (without a normalisation) can be implemented as follows. First, we measure O_m and construct operators $M_m^{i'_m i_m} = \langle\varphi^{i'_m}| O_m |\varphi^{i_m}\rangle$. Note that each M_m is a 2×2 Hermitian matrix when O_m is Hermitian. Then, since M_m is Hermitian, we can measure an expectation value of $\bigotimes_{m=1}^{k} M_m$ for the state $|\psi\rangle$, which is equal to $\langle O\rangle$.

The approach allows for simulations beyond the scale of quantum hardware. For example, the energy and the spin-spin correlation functions of electrons can be calculated with this approach. However, the approach has a serious problem for expanding the range of applications: it can only be applied to the calculation of the expectation value of observables. In other words, there is a problem in the approach when the contracted operator M_m is non-Hermitian. Hereinafter, we denote the Hermitian and non-Hermitian contracted operators as M_m and N_m, respectively. The reason for the problem is that the number of terms to be measured increases exponentially with k when $\bigotimes_{m=1}^{k} N_m$ is calculated naively. Specifically, the non-Hermitian operators are decomposed into the sums of Pauli operators, as in $\bigotimes_{m=1}^{k} N_m = \bigotimes_{m=1}^{k}(h_{Im} I_m + h_{Xm} X_m + h_{Ym} Y_m + h_{Zm} Z_m)$, where I_m is an identity operator, X_m, Y_m and Z_m are Pauli operators which act on m-th qubit, and $h_\alpha (\alpha \in \{I_m, X_m, Y_m, Z_m\})$ are corresponding coefficients, with up to 4^k terms appearing. One example where the problem occurs is in the calculation of the transition amplitude related to the Green's functions and the photon emissions/absorptions [31, 32]. The overlap of two quantum states, which is used as subroutines in many algorithms [33–36], is a special case of the transition amplitude. Thus, the difficulty of computing the expectation value of a non-Hermitian operator limits the applicability of the hybrid tensor network approach.

In this study, we propose a method for calculating transition amplitudes by the hybrid tensor network approach. The main point of the method is the treatment of tensor products of non-Hermitian operators. In the naive calculation, the exponential number of terms in $\bigotimes_{m=1}^{k} N_m$ will appear. We propose two ways to avoid the problem. One is a Monte-Carlo contraction method and the other is a singular value decomposition (SVD) contraction method, and the second method is the main proposal in this paper. Although the first method can avoid measuring all the terms whose number increases exponentially with k, the second method is exponentially more efficient than the first one in terms of the sampling cost.

In the following, we firstly introduce the overview of a quantum-quantum tree-tensor network [17] for obtaining the expectation values of observables in Sec. 2. Then, the method of calculating transition amplitudes and overlaps is shown in Sec. 3, especially we discuss the contraction of quantum tensors in subsystems in Sec. 3.1 and the contraction of non-Hermitian matrices in Sec. 3.2. We discuss the future application of the method in Sec. 4.

2. Overview of hybrid tensor network

We present an overview of the hybrid tensor network

simulation on the state described by the tensor network in Eq. (2). Letting the observable O as $O = \bigotimes_{m=1}^{k} O_m$ and $O_m = \bigotimes_{r=1}^{n} O_{mr}$ $(r = 1, 2, \ldots, n)$, the expectation value of the observable including a normalisation constant can be described as

$$\begin{aligned}\langle O\rangle &= \frac{1}{A^2}\langle\psi_{HT}|\, O\,|\psi_{HT}\rangle \\ &= \frac{1}{A^2}\sum_{\vec{i}'\ \vec{i}} \psi^*_{\vec{i}'}\psi_{\vec{i}} \prod_{m=1}^{k} M_m^{i'_m i_m}\end{aligned} \tag{3}$$

and

$$\begin{aligned}A &= \sqrt{\langle\psi_{HT}|\psi_{HT}\rangle} \\ &= \sqrt{\sum_{\vec{i}'\ \vec{i}} \psi^*_{\vec{i}'}\psi_{\vec{i}} \prod_{m=1}^{k} M_{Am}^{i'_m i_m}},\end{aligned} \tag{4}$$

where A is a normalization constant, $\vec{i} = (i_1, i_2, \ldots, i_k)$ with i_m taking either 0 or 1, $M_m^{i'_m i_m} = \langle\varphi^{i'_m}|\, O_m\,|\varphi^{i_m}\rangle$, and $M_{Am}^{i'_m i_m} = \langle\varphi^{i'_m}|\varphi^{i_m}\rangle$. $M_m^{i'_m i_m}$ $(M_{Am}^{i'_m i_m})$ is the element of the 2×2 matrix M_m (M_{Am}). When O_m is assumed to be an observable, i.e., a Hermitian operator, M_m also becomes a Hermitian operator. M_{Am} is a Hermitian operator since M_{Am} is a special case of $O_m = I_m$ in M_m, where I_m is the identity operator.

The procedure for constructing M_m and M_{Am} depends on how the indices i_m of the wave function $|\varphi^{i_m}\rangle$ are mapped. We assume two cases of the mapping; one case is where the indices i_m are mapped to unitary gates, i.e., $|\varphi^{i_m}\rangle = U_{Cm}^{i_m}|0\rangle^{\otimes n}$, and another case is where the indices i_m are mapped to initial wave function as $|\varphi^{i_m}\rangle = U_{Cm}\,|i_m\rangle\,|0\rangle^{\otimes n-1}$, where $U_{Cm}^{i_m}$ and U_{Cm} are unitary operators with polynomial depth in the m-th subsystem. The second case can be regard as a special example in the first case since $|\varphi^{i_m}\rangle = U_{Cm}\,|i_m\rangle\,|0\rangle^{\otimes n-1} = U_{Cm}(X_1)^{i_m}\,|0\rangle^{\otimes n}$ and we can think of $U_{Cm}(X_1)^{i_m}$ as $U_{Cm}^{i_m}$, where X_1 is a Pauli X operator which acts on the first qubit. Note that the first method needs a Hadamard test circuit while M_m and M_{Am} can be efficiently constructed via direct measurements in the second case as will be described later.

We first consider the construction of M_m in the case of $|\varphi^{i_m}\rangle = U_{Cm}^{i_m}|0\rangle^{\otimes n}$. Since the procedure for measuring the diagonal elements is relatively straightforward, we focus on the measurement of non-diagonal elements. Figure 2(a) shows a quantum circuit to obtain the matrix element $M_m^{i'_m i_m}$. The procedure to construct M_m is as follows. First, we prepare initial states. We use the Hadamard test to prepare $|\varphi^{i'_m}\rangle = U_{Cm}^{i'_m}|0\rangle^{\otimes n}$ and $|\varphi^{i_m}\rangle = U_{Cm}^{i_m}|0\rangle^{\otimes n}$. The ancilla qubit is initialised to $\frac{|0\rangle+e^{i\alpha}|1\rangle}{\sqrt{2}}$, where α is the phase. We set $\alpha = 0$ $(\alpha = \frac{\pi}{2})$ to obtain real (imaginary) part of $M_m^{i'_m i_m}$. Since M_m is an

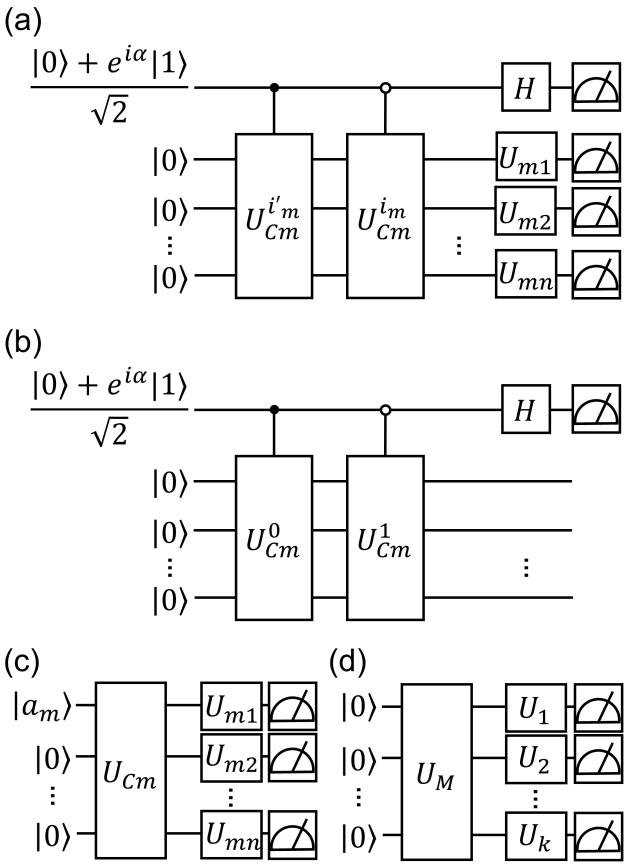

図 2 The quantum circuits for obtaining $\langle O\rangle$. In figures (a) and (b), the topmost line represents an ancilla qubit and the other lines represent system qubits, and in figures (c) and (d), all lines represent system qubits. Real and imaginary components are obtained by setting $\alpha = 0$ and $\alpha = \frac{\pi}{2}$, respectively. A white (black) circle in a controlled gate means that a unitary operation is performed on the target qubits when the control qubit is $|0\rangle$ ($|1\rangle$). (a) A quantum circuit to construct M_m in the case of $|\varphi^{i_m}\rangle = U_{Cm}^{i_m}|0\rangle^{\otimes n}$. (b) A quantum circuit to construct M_{Am} in the case of $|\varphi^{i_m}\rangle = U_{Cm}^{i_m}|0\rangle^{\otimes n}$. (c) A quantum circuit to construct M_m in the case of $|\varphi^{i_m}\rangle = U_{Cm}\,|i_m\rangle\,|0\rangle^{\otimes n-1}$. $|a_m\rangle$ takes $|0\rangle$, $|1\rangle$, $|+\rangle$ and $|+y\rangle$. (d) A quantum circuit to measure M_m and M_{Am}.

Hermitian matrix, only measurements of $\mathrm{Re}(M_m^{01})$, and $\mathrm{Im}(M_m^{01})$ are required. Then, we measure on a computational basis. We used the fact that O_{mr} is a Hermitian operator and can have a spectral decomposition as $O_{mr} = U_{mr}^{\dagger} D_{mr} U_{mr}$, where U_{mr} is a unitary matrix and D_{mr} is a diagonal matrix. Also, we assign elements of D_{mr} as the measured value. More concretely, denoting $D_{mr} = \mathrm{diag}[\lambda_{j_r=0}^{(mr)}, \lambda_{j_r=1}^{(mr)}]$, the measured value is computed as $\prod_{r=1}^{n}\lambda_{j_r}^{(mr)}$ corresponding to the measured outcome $\vec{j} = (j_1, j_2, \ldots, j_n)$.

We explain how to construct M_{Am}. Figure 2(b) shows the circuit to construct M_{Am}. In the case of $|\varphi^{i_m}\rangle =$

$U_{Cm}^{i_m}|0\rangle^{\otimes n}$, since $|\varphi^{i_m}\rangle$ is non-orthogonal to each other, we have $A \neq 1$. Therefore, calculations of M_{Am} are required. The circuit in Fig. 2(b) is a modified version of that in Fig. 2(a) except that the system measurements are not necessary; we can construct M_{Am} using the same construction procedure as M_m.

Next, we assume the case of $|\varphi^{i_m}\rangle = U_{Cm}|i_m\rangle|0\rangle^{\otimes n-1}$. In this case, we can obtain all the elements of M_m only from the results of direct measurements. Figure 2(c) shows a quantum circuit to construct M_m. The initial states are set to $|a_m\rangle|0\rangle^{\otimes n-1}$, where $|a_m\rangle$ takes four states as $|0\rangle$, $|1\rangle$, $|+\rangle$ and $|+y\rangle$. Then M_m can be obtained using the corresponding measurement results. Refer to Appendix A.1 for the detail of the procedure. Also, since $|\varphi^{i_m}\rangle$ is orthogonal, $A = 1$ and the calculation of M_{Am} is not required.

Finally, we show the procedure to obtain $\langle\psi_{HT}|O|\psi_{HT}\rangle$, which can be implemented by contracting M_m and M_{A_m}. Now, denoting $|\psi\rangle = \sum_{\vec{i}}\psi_{\vec{i}}|\vec{i}\rangle = \sum_{i_1,i_2,\ldots,i_k}\psi_{i_1,i_2,\ldots,i_k}|i_1 i_2 \ldots i_k\rangle$, we can rewrite Eq. (3) as

$$\begin{aligned} A^2\langle O\rangle &= \langle\psi|\bigotimes_{m=1}^{k} M_m|\psi\rangle \\ &= \langle\psi|\bigotimes_{m=1}^{k} U_m^\dagger D_m U_m|\psi\rangle, \end{aligned} \tag{5}$$

where we used the fact that M_m is a Hermitian operator and can have a spectral decomposition as $M_m = U_m^\dagger D_m U_m$. Figure 2(d) shows a quantum circuit to measure M_m. Henceforth, we assume $|\psi\rangle = U_M|0\rangle^{\otimes n}$, where U_M is a unitary operator with polynomial depth. We can compute $A^2\langle O\rangle$ by applying U_m, measuring in a computational basis, and assigning elements of D_m as the measured value. More concretely, denoting $D_m = \mathrm{diag}[\lambda_{i_m=0}^{(m)}, \lambda_{i_m=1}^{(m)}]$, the measured value is computed as $\prod_{m=1}^{k}\lambda_{i_m}^{(m)}$ corresponding to the measured outcome $\vec{i} = (i_1, i_2, \ldots, i_k)$. In a similar procedure, we can measure A^2 by contracting M_{A_m}; hence we can obtain $\langle O\rangle$.

3. Calculation of transition amplitudes and overlaps

We describe the measurement of transition amplitudes with the hybrid tensor network approach. The difference from Sec. 2 is that we need to contract a non-Hermitian operator N_m.

3.1 Contraction of quantum tensors in subsystems

Letting two different states represented by quantum-quantum tensor network as $|\psi_{HT}^{(1)}\rangle$ and $|\psi_{HT}^{(2)}\rangle$, N_m appears in calculations of $\langle\psi_{HT}^{(1)}|O|\psi_{HT}^{(2)}\rangle$ in transition amplitudes or $\langle\psi_{HT}^{(1)}|\psi_{HT}^{(2)}\rangle$ in overlaps.

To begin with, we consider the calculation of the transition amplitude because the overlap is a special case of $O = I$ in the transition amplitude, where I is the identity operator. We comment on the overlap at the end of this section. The transition amplitude T can be defined as

$$\begin{aligned} T &= \frac{1}{A^{(1)}A^{(2)}}\langle\psi_{HT}^{(1)}|O|\psi_{HT}^{(2)}\rangle \\ &= \frac{1}{A^{(1)}A^{(2)}}\sum_{\vec{i}',\,\vec{i}}\psi_{\vec{i}'}^{(1)*}\psi_{\vec{i}}^{(2)}\prod_{m=1}^{k}N_m^{i'_m i_m} \\ &= \frac{1}{A^{(1)}A^{(2)}}\langle\psi^{(1)}|\bigotimes_{m=1}^{k}N_m|\psi^{(2)}\rangle, \end{aligned} \tag{6}$$

where $A^{(l)}$ $(l = 1, 2)$ is a normalisation constant corresponding to $|\psi_{HT}^{(l)}\rangle$, $\vec{i} = (i_1, i_2, \ldots, i_k)$, N_m is a 2×2 matrix with elements of $N_m^{i'_m i_m} = \langle\varphi^{i'_m(1)}|O_m|\varphi^{i_m(2)}\rangle$, and $|\psi^{(l)}\rangle = \sum_{\vec{i}}\psi_{\vec{i}}^{(l)}|\vec{i}\rangle = \sum_{i_1,i_2,\ldots,i_k}\psi_{i_1,i_2,\ldots,i_k}^{(l)}|i_1 i_2 \ldots i_k\rangle$. The notations are the same as in Eqs. (3), (4) and (5), except for the superscript (l), which corresponds to $|\psi_{HT}^{(l)}\rangle$. The reason that N_m is a non-Hermitian matrix comes from the fact that $(N_m^{i'_m i_m})^* \neq N_m^{i_m i'_m}$. Since the procedure for calculating $A^{(l)}$ is the same as the procedure for A in the previous section, we will not discuss $A^{(l)}$ in the following.

We first consider the case of $|\varphi^{i_m(l)}\rangle = U_{Cm}^{i_m(l)}|0\rangle^{\otimes n}$. Figure 3(a) shows the quantum circuit for constructing N_m. The flow of constructing N_m is similar to that of M_m. However, since N_m is a 2×2 non-Hermitian matrix with elements of complex numbers, eight types of measurements are required to construct N_m. Next, we consider the case of $|\varphi^{i_m(l)}\rangle = U_{Cm}^{(l)}|i_m\rangle|0\rangle^{\otimes n-1}$. Figure 3(b) shows a quantum circuit to obtain the matrix element $N_m^{i'_m i_m}$. Specifically, the wave function is initialized by using one of the four types of unitary gates U_{init} in lower panel of Fig. 3(b) to prepare the initial states $|i'_m\rangle|0\rangle^{\otimes n-1}$ and $|i_m\rangle|0\rangle^{\otimes n-1}$. The subsequent process is the same as the case of $|\varphi^{i_m(l)}\rangle = U_{Cm}^{i_m(l)}|0\rangle^{\otimes n}$.

When calculating the overlap S, i.e., the case of $O = I$ in Eq. (6), only the circuits to construct N_m (Fig. 3(a) and (b)) differ from the cases of the transition amplitude. We show the circuits in the cases of $|\varphi^{i_m(l)}\rangle = U_{Cm}^{i_m(l)}|0\rangle^{\otimes n}$ and $|\varphi^{i_m(l)}\rangle = U_{Cm}^{(l)}|i_m\rangle|0\rangle^{\otimes n-1}$ in Fig. 3(c) and (d), which are the same quantum circuits as Fig. 3(a) and

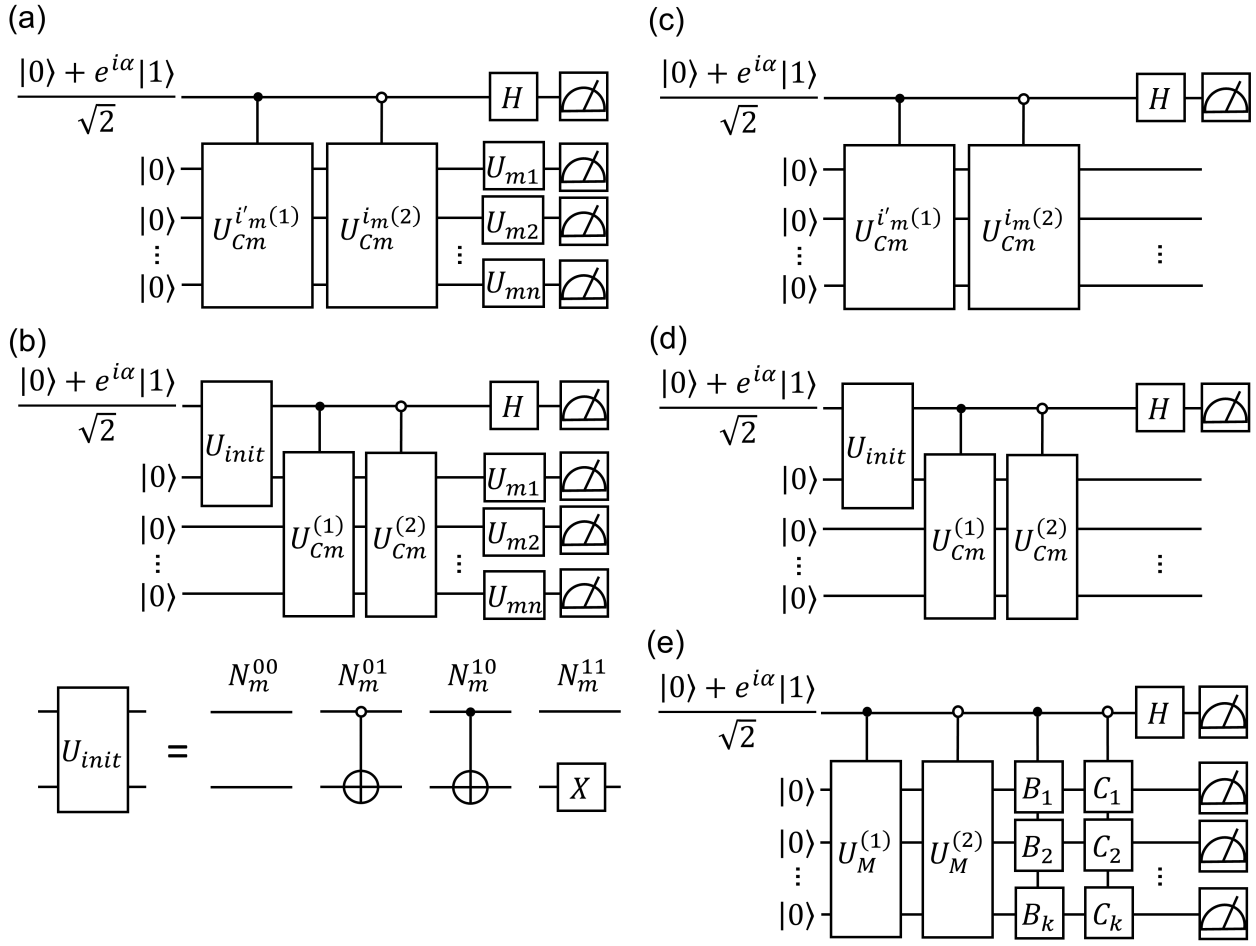

図 3 The quantum circuits for obtaining transition amplitudes and overlaps. In all the figures, the topmost line represents an ancilla qubit and the other lines represent system qubits. Real and imaginary components are obtained by setting $\alpha = 0$ and $\alpha = \frac{\pi}{2}$, respectively. A white (black) circle in a controlled gate means that a unitary operation is performed on the target qubits when the control qubit is $|0\rangle$ ($|1\rangle$). (a) A quantum circuit to construct N_m for calculating transition amplitudes in the case of $|\varphi^{i_m(l)}\rangle = U_{Cm}^{i_m(l)} |0\rangle^{\otimes n}$. (b) A quantum circuit to construct N_m for calculating transition amplitudes in the case of $|\varphi^{i_m(l)}\rangle = U_{Cm}^{(l)} |i_m\rangle |0\rangle^{\otimes n-1}$. (c) A quantum circuit to construct N_m for calculating overlaps in the case of $|\varphi^{i_m(l)}\rangle = U_{Cm}^{i_m(l)} |0\rangle^{\otimes n}$. (d) A quantum circuit to construct N_m for calculating overlaps in the case of $|\varphi^{i_m(l)}\rangle = U_{Cm}^{(l)} |i_m\rangle |0\rangle^{\otimes n-1}$. (e) A quantum circuit to measure N_m for calculating transition amplitudes or overlaps.

(b) except that measurements of system qubits are not involved.

3.2 Contraction of non-Hermitian matrices

The next step is to calculate $\langle\psi^{(1)}| \bigotimes_{m=1}^{k} N_m |\psi^{(2)}\rangle$ for 2×2 non-Hermitian matrices N_m. We describe two methods for contraction: a Monte-Carlo contraction method and an SVD contraction method. In this section, we describe the SVD contraction method because it is more efficient than the Monte-Carlo contraction method in terms of the sampling cost. Refer to Appendix A.2 for details of the Monte-Carlo contraction method.

We describe how to perform the SVD contraction method. In the method, we perform SVD $N_m = B_m^\dagger D'_m C_m$ for each N_m, that is, $\bigotimes_{m=1}^{k} N_m = \bigotimes_{m=1}^{k} B_m^\dagger D'_m C_m$, where B_m and C_m are unitary matrices and D'_m is a diagonal matrix with non-negative elements. $\langle\psi^{(1)}| \bigotimes_{m=1}^{k} N_m |\psi^{(2)}\rangle$ can be described as

$$\begin{aligned}&\langle\psi^{(1)}|\bigotimes_{m=1}^{k}N_m\,|\psi^{(2)}\rangle\\&=2(\prod_{m=1}^{k}\|N_m\|_{op})\cdot\frac{1}{2}\times\big[\mathrm{Re}(\langle\psi^{(1)}|\bigotimes_{m=1}^{k}B_m^{\dagger}d'^{(m)}C_m\,|\psi^{(2)}\rangle)\\&+i\mathrm{Im}(\langle\psi^{(1)}|\bigotimes_{m=1}^{k}B_m^{\dagger}d'^{(m)}C_m\,|\psi^{(2)}\rangle)\big],\end{aligned}\tag{7}$$

where $\|A\|_{op}$ is the operator norm of an operator A, $d'^{(m)} = D'_m/\|N_m\|_{op}$. We can assume $d'^{(m)} = \mathrm{diag}[\tilde{\lambda}'^{(m)}_{i_m=0}, \tilde{\lambda}'^{(m)}_{i_m=1}] = \mathrm{diag}[1, \tilde{\lambda}'^{(m)}_{i_m=1}]$, where $\tilde{\lambda}'^{(m)}_{i_m=0} \geq \tilde{\lambda}'^{(m)}_{i_m=1}$, $\tilde{\lambda}'^{(m)}_{i_m=0} = 1$, and $\tilde{\lambda}'^{(m)}_{i_m=1}$ takes a value in a range $[0, 1]$, without loss of generality.

Figure 3(e) shows the circuit for measuring $\langle\psi^{(1)}|\bigotimes_{m=1}^{k}N_m\,|\psi^{(2)}\rangle$ by the SVD contraction method. We can compute $\langle\psi^{(1)}|\bigotimes_{m=1}^{k}N_m\,|\psi^{(2)}\rangle$ as follows. We implement a Hadamard test circuit for $\bigotimes_{m=1}^{k}B_m^{\dagger}d'^{(m)}C_m$ for obtaining the real or imaginary part of $\langle\psi^{(1)}|\bigotimes_{m=1}^{k}N_m\,|\psi^{(2)}\rangle$ with probability $1/2$ by changing the phase of the ancilla qubit. We define $\mu_s = 2(\prod_{m=1}^{k}\|N_m\|_{op})(\prod_{m=1}^{k}\tilde{\lambda}'^{(m)}_{i_{ms}})b_s$ and $\mu_s = 2i(\prod_{m=1}^{k}\|N_m\|_{op})(\prod_{m=1}^{k}\tilde{\lambda}'^{(m)}_{i_{ms}})b_s$ in the case of measurements of real and imaginary part, respectively, where $i_{ms} \in \{0, 1\}$ and $b_s \in \{-1, 1\}$ are the measurement outcomes of the system and ancilla qubits in the s-th measurement, respectively. Then the sample average of μ_s approximates $\langle\psi^{(1)}|\bigotimes_{m=1}^{k}N_m\,|\psi^{(2)}\rangle$.

Letting $\bar{x}$ denote the sample average of a random variable x, $\mathrm{E}[x]$ denote the expected value of x, and $\bar{\mu}_s$ approximate $\langle\psi^{(1)}|\bigotimes_{m=1}^{k}N_m\,|\psi^{(2)}\rangle$. Denoting the number of measurements as N_{SVD} and assuming $\forall m\ \|N_m\|_{op} = \|N_{const}\|_{op}$, we have

$$\mathrm{E}[|\bar{\mu}_s - \langle\psi^{(1)}|\bigotimes_{m=1}^{k}N_m\,|\psi^{(2)}\rangle\,|] = O\Big(\frac{(\|N_{const}\|_{op})^k}{\sqrt{N_{SVD}}}\Big).\tag{8}$$

Thus, we have

$$N_{SVD} = O\Big(\frac{(\|N_{const}\|_{op})^{2k}}{\varepsilon^2}\Big)\tag{9}$$

for the required accuracy ε. We remark that this method is exponentially more efficient than the Monte-Carlo contraction method in terms of the sampling cost. Refer to Appendix A.3 for details.

We mention that N_{SVD} is expected not to increase exponentially with k if n is large enough. Here, we consider the case where the measured observable O is a product of Pauli operators because in the conventional variational quantum eigensolver (VQE) [11] scenario, we decompose the Hermitian operator of interest into a linear combination of the polynomial number of products of Pauli operators with the system size. We numerically generate four types of $2^n \times 2^n$ random unitary matrices, $U^{0(1)}$, $U^{1(1)}$, $U^{0(2)}$, and $U^{1(2)}$, and a product of random Pauli operators, O_{rand}, create a 2×2 matrix N_{const} consisting of elements $N^{i'i}_{const} = \langle 0|^{\otimes n} U^{i'(1)\dagger} O_{rand} U^{i(2)}\,|0\rangle^{\otimes n}$, where i' and i take 0 or 1. Then, we evaluate average values of $\|N_{const}\|_{op}$ obtained using $10,000$ samples of N_{const}. As a result, we obtained $\|N_{const}\|_{op} < 1$ including error bars when $n \geq 3$ (See Appendix A.3 for details). Therefore, if n is large enough, $N_{SVD} \leq O(1/\varepsilon^2)$ will be valid.

Besides, we note that in the case of $|\varphi^{i_m(l)}\rangle = U^{(l)}_{Cm}\,|i_m\rangle\,|0\rangle^{\otimes n-1}$, $N_{SVD} \leq O(1/\varepsilon^2)$ is strictly satisfied regardless of n. In this case, since N_m can be regarded as a submatrix of the unitary matrix $U^{(1)\dagger}_{Cm} O_m U^{(2)}_{Cm}$ as $N^{i'_m i_m}_m = \langle i'_m|\,\langle 0|^{\otimes n-1} U^{(1)\dagger}_{Cm} O_m U^{(2)}_{Cm}\,|i_m\rangle\,|0\rangle^{\otimes n-1}$, we have $\|N_m\|_{op} \leq \|O_m\|_{op}$. Thus, because we are assuming $\|O_m\|_{op} = 1$ here, we have $N_{SVD} \leq O(1/\varepsilon^2)$ regardless of n.

4. Conclusion

In this paper, we proposed a method to calculate transition amplitudes using the hybrid tensor network. When the approach is applied to the calculations of transition amplitudes naively, the contracted operators become non-Hermitian, and the number of terms to be measured increases exponentially. We proposed a method to obtain the expectation value without increasing the number of terms exponentially by using the singular value decomposition and the Hadamard test. We remark that our theory can be easily generalized to the cases with a mixture of classical and quantum tensors called quantum-classical and classical-quantum tree-tensor networks, and those with deeper tree structures. We also note that we can easily extend the scenario to the case where the measured operator O is a tensor product of non-Hermitian operators by using the SVD contraction method. This study significantly expands the applicability of the hybrid tensor network.

Future work includes the application of our method to algorithms related to hybrid tensor networks. For example, Deep VQE [18, 19], which is a large-scale computational algorithm for NISQ devices based on the divide and conquer method, can be treated in the framework of hybrid tensor networks in theory. By applying the proposed method to such algorithms, we can extend the range of

applications to various large-scale quantum algorithms.

謝 辞 This work is supported by PRESTO, JST, Grant No. JPMJPR1916; ERATO, JST, Grant No. JPMJER1601; CREST, JST, Grant No. JPMJCR1771; Moonshot R&D, JST, Grant No. JPMJMS2061; MEXT Q-LEAP Grant No. JPMXS0120319794 and JPMXS0118068682. S.E acknowledges useful discussions with Jinzhao Sun and Xiao Yuan.

参考文献

[1] K. Bharti, A. Cervera-Lierta, T. H. Kyaw, T. Haug, S. Alperin-Lea, A. Anand, M. Degroote, H. Heimonen, J. S. Kottmann, T. Menke, W.-K. Mok, S. Sim, L.-C. Kwek, and A. Aspuru-Guzik, "Noisy intermediate-scale quantum (NISQ) algorithms," Jan. 2021, arXiv:2101.08448.

[2] M. Cerezo, A. Arrasmith, R. Babbush, S. C. Benjamin, S. Endo, K. Fujii, J. R. McClean, K. Mitarai, X. Yuan, L. Cincio, and P. J. Coles, "Variational quantum algorithms," Dec. 2020, arXiv:2012.09265.

[3] Y. Cao, J. Romero, J. P. Olson, M. Degroote, P. D. Johnson, M. Kieferová, I. D. Kivlichan, T. Menke, B. Peropadre, N. P. D. Sawaya, S. Sim, L. Veis, and A. Aspuru-Guzik, "Quantum chemistry in the age of quantum computing," *Chem. Rev.*, vol. 119, pp. 10856–10915, Oct. 2019.

[4] S. Endo, Z. Cai, S. C. Benjamin, and X. Yuan, "Hybrid Quantum-Classical algorithms and quantum error mitigation," *J. Phys. Soc. Jpn.*, vol. 90, p. 032001, Mar. 2021.

[5] Y. Shikano, H. C. Watanabe, K. M. Nakanishi, and Y.-Y. Ohnishi, "Post-Hartree-Fock method in quantum chemistry for quantum computer," Nov. 2020, arXiv:2011.01544.

[6] S. McArdle, S. Endo, A. Aspuru-Guzik, S. C. Benjamin, and X. Yuan, "Quantum computational chemistry," *Rev. Mod. Phys.*, vol. 92, p. 015003, Mar. 2020.

[7] B. Bauer, S. Bravyi, M. Motta, and G. Kin-Lic Chan, "Quantum algorithms for quantum chemistry and quantum materials science," *Chem. Rev.*, vol. 120, pp. 12685–12717, Nov. 2020.

[8] F. Arute, K. Arya, R. Babbush, D. Bacon, J. C. Bardin, R. Barends, R. Biswas, S. Boixo, F. G. S. L. Brandao, D. A. Buell, B. Burkett, Y. Chen, Z. Chen, B. Chiaro, R. Collins, W. Courtney, A. Dunsworth, E. Farhi, B. Foxen, A. Fowler, C. Gidney, M. Giustina, R. Graff, K. Guerin, S. Habegger, M. P. Harrigan, M. J. Hartmann, A. Ho, M. Hoffmann, T. Huang, T. S. Humble, S. V. Isakov, E. Jeffrey, Z. Jiang, D. Kafri, K. Kechedzhi, J. Kelly, P. V. Klimov, S. Knysh, A. Korotkov, F. Kostritsa, D. Landhuis, M. Lindmark, E. Lucero, D. Lyakh, S. Mandrà, J. R. McClean, M. McEwen, A. Megrant, X. Mi, K. Michielsen, M. Mohseni, J. Mutus, O. Naaman, M. Neeley, C. Neill, M. Y. Niu, E. Ostby, A. Petukhov, J. C. Platt, C. Quintana, E. G. Rieffel, P. Roushan, N. C. Rubin, D. Sank, K. J. Satzinger, V. Smelyanskiy, K. J. Sung, M. D. Trevithick, A. Vainsencher, B. Villalonga, T. White, Z. J. Yao, P. Yeh, A. Zalcman, H. Neven, and J. M. Martinis, "Quantum supremacy using a programmable superconducting processor," *Nature*, vol. 574, pp. 505–510, Oct. 2019.

[9] H.-S. Zhong, H. Wang, Y.-H. Deng, M.-C. Chen, L.-C. Peng, Y.-H. Luo, J. Qin, D. Wu, X. Ding, Y. Hu, P. Hu, X.-Y. Yang, W.-J. Zhang, H. Li, Y. Li, X. Jiang, L. Gan, G. Yang, L. You, Z. Wang, L. Li, N.-L. Liu, C.-Y. Lu, and J.-W. Pan, "Quantum computational advantage using photons," *Science*, vol. 370, pp. 1460–1463, Dec. 2020.

[10] J. Preskill, "Quantum computing in the NISQ era and beyond," *Quantum*, vol. 2, p. 79, Aug. 2018.

[11] A. Peruzzo, J. McClean, P. Shadbolt, M.-H. Yung, X.-Q. Zhou, P. J. Love, A. Aspuru-Guzik, and J. L. O'Brien, "A variational eigenvalue solver on a photonic quantum processor," *Nat. Commun.*, vol. 5, p. 4213, July 2014.

[12] A. Kandala, A. Mezzacapo, K. Temme, M. Takita, M. Brink, J. M. Chow, and J. M. Gambetta, "Hardware-efficient variational quantum eigensolver for small molecules and quantum magnets," *Nature*, vol. 549, pp. 242–246, Sept. 2017.

[13] K. Temme, S. Bravyi, and J. M. Gambetta, "Error mitigation for Short-Depth quantum circuits," *Phys. Rev. Lett.*, vol. 119, p. 180509, Nov. 2017.

[14] S. Endo, S. C. Benjamin, and Y. Li, "Practical quantum error mitigation for Near-Future applications," *Phys. Rev. X*, vol. 8, p. 031027, July 2018.

[15] A. Kandala, K. Temme, A. D. Córcoles, A. Mezzacapo, J. M. Chow, and J. M. Gambetta, "Error mitigation extends the computational reach of a noisy quantum processor," *Nature*, vol. 567, pp. 491–495, Mar. 2019.

[16] R. Takagi, "Optimal resource cost for error mitigation," June 2020, arXiv:2006.12509.

[17] X. Yuan, J. Sun, J. Liu, Q. Zhao, and Y. Zhou, "Quantum simulation with hybrid tensor networks," July 2020, arXiv:2007.00958.

[18] K. Fujii, K. Mitarai, W. Mizukami, and Y. O. Nakagawa, "Deep variational quantum eigensolver: a divide-and-conquer method for solving a larger problem with smaller size quantum computers," July 2020, arXiv:2007.10917.

[19] K. Mizuta, M. Fujii, S. Fujii, K. Ichikawa, Y. Imamura, Y. Okuno, and Y. O. Nakagawa, "Deep variational quantum eigensolver for excited states and its application to quantum chemistry calculation of periodic materials," Apr. 2021, arXiv:2104.00855.

[20] T. Takeshita, N. C. Rubin, Z. Jiang, E. Lee, R. Babbush, and J. R. McClean, "Increasing the representation accuracy of quantum simulations of chemistry without extra quantum resources," *Phys. Rev. X*, vol. 10, p. 011004, Jan. 2020.

[21] T. Yamazaki, S. Matsuura, A. Narimani, A. Saidmuradov, and A. Zaribafiyan, "Towards the practical application of Near-Term quantum computers in quantum chemistry simulations: A problem decomposition approach," June 2018, arXiv:1806.01305.

[22] N. P. Bauman, E. J. Bylaska, S. Krishnamoorthy, G. H. Low, N. Wiebe, C. E. Granade, M. Roetteler, M. Troyer, and K. Kowalski, "Downfolding of many-body hamiltonians using active-space models: Extension of the sub-system embedding sub-algebras approach to unitary coupled cluster formalisms," *J. Chem. Phys.*, vol. 151, p. 014107, July 2019.

[23] J. S. Kottmann, P. Schleich, T. Tamayo-Mendoza, and A. Aspuru-Guzik, "Reducing qubit requirements while maintaining numerical precision for the variational quantum eigensolver: A Basis-Set-Free approach," *J. Phys. Chem. Lett.*, vol. 12, pp. 663–673, Jan. 2021.

[24] W. Huggins, P. Patil, B. Mitchell, K. Birgitta Whaley, and E. Miles Stoudenmire, "Towards quantum machine learning with tensor networks," *Quantum Sci. Technol.*, vol. 4, p. 024001, Jan. 2019.
[25] I. Cong, S. Choi, and M. D. Lukin, "Quantum convolutional neural networks," *Nat. Phys.*, vol. 15, pp. 1273–1278, Aug. 2019.
[26] I. H. Kim, "Holographic quantum simulation," Feb. 2017, arXiv:1702.02093.
[27] J.-G. Liu, Y.-H. Zhang, Y. Wan, and L. Wang, "Variational quantum eigensolver with fewer qubits," *Phys. Rev. Research*, vol. 1, p. 023025, Sept. 2019.
[28] M. Foss-Feig, D. Hayes, J. M. Dreiling, C. Figgatt, J. P. Gaebler, S. A. Moses, J. M. Pino, and A. C. Potter, "Holographic quantum algorithms for simulating correlated spin systems," May 2020, arXiv:2005.03023.
[29] A. Eddins, M. Motta, T. P. Gujarati, S. Bravyi, A. Mezzacapo, C. Hadfield, and S. Sheldon, "Doubling the size of quantum simulators by entanglement forging," Apr. 2021, arXiv:2104.10220.
[30] U. Schollwöck, "The density-matrix renormalization group in the age of matrix product states," *Ann. Phys.*, vol. 326, pp. 96–192, Jan. 2011.
[31] S. Endo, I. Kurata, and Y. O. Nakagawa, "Calculation of the green's function on near-term quantum computers," *Phys. Rev. Research*, vol. 2, p. 033281, Aug. 2020.
[32] Y. Ibe, Y. O. Nakagawa, N. Earnest, T. Yamamoto, K. Mitarai, Q. Gao, and T. Kobayashi, "Calculating transition amplitudes by variational quantum deflation," Feb. 2020, arXiv:2002.11724.
[33] J. Romero, J. P. Olson, and A. Aspuru-Guzik, "Quantum autoencoders for efficient compression of quantum data," *Quantum Sci. Technol.*, vol. 2, p. 045001, Aug. 2017.
[34] R. LaRose, A. Tikku, É. O'Neel-Judy, L. Cincio, and P. J. Coles, "Variational quantum state diagonalization," *npj Quantum Information*, vol. 5, pp. 1–10, June 2019.
[35] T. Jones, S. Endo, S. McArdle, X. Yuan, and S. C. Benjamin, "Variational quantum algorithms for discovering hamiltonian spectra," *Phys. Rev. A*, vol. 99, p. 062304, June 2019.
[36] O. Higgott, D. Wang, and S. Brierley, "Variational quantum computation of excited states," *Quantum*, vol. 3, p. 156, July 2019.

付　　録

A.1 The construction of M_m in the case where indices i_m are mapped to initial wave functions

We explain the procedure for the construction of M_m in the case of $|\varphi^{i_m}\rangle = U_{Cm}|i_m\rangle|0\rangle^{\otimes n-1}$ using the circuit in Fig. 2(c). The diagonal elements, M_m^{00} and M_m^{11}, can be easily obtained by measuring the expectation values of O_m for $|\varphi^{i_m=0}\rangle$ and $|\varphi^{i_m=1}\rangle$ because $M_m^{00} = \langle\varphi^{i_m=0}|O_m|\varphi^{i_m=0}\rangle$ and $M_m^{11} = \langle\varphi^{i_m=1}|O_m|\varphi^{i_m=1}\rangle$, respectively. We can also obtain non-diagonal elements by combining four types of measurement results. By setting $|+^{(m)}\rangle = (|\varphi^{i_m=0}\rangle + |\varphi^{i_m=1}\rangle)/\sqrt{2}$ and $|+y^{(m)}\rangle = (|\varphi^{i_m=0}\rangle + i|\varphi^{i_m=1}\rangle)/\sqrt{2}$, we have

$$\langle+^{(m)}|O_m|+^{(m)}\rangle = \frac{1}{2}(M_m^{00} + M_m^{01} + M_m^{10} + M_m^{11}) \tag{A.1}$$

and

$$\langle+y^{(m)}|O_m|+y^{(m)}\rangle = \frac{1}{2}(M_m^{00} + iM_m^{01} - iM_m^{10} + M_m^{11}). \tag{A.2}$$

Then, we can obtain the non-diagonal elements by

$$\begin{aligned} M_m^{01} = &\frac{i-1}{2}\langle\varphi^{i_m=0}|O_m|\varphi^{i_m=0}\rangle \\ &+ \frac{i-1}{2}\langle\varphi^{i_m=1}|O_m|\varphi^{i_m=1}\rangle \\ &+ \langle+^{(m)}|O_m|+^{(m)}\rangle \\ &- i\langle+y^{(m)}|O_m|+y^{(m)}\rangle \end{aligned} \tag{A.3}$$

and $M_m^{10} = M_m^{01*}$.

A.2 Monte-Carlo contraction method

In this section, we introduce a Monte-Carlo contraction method and discuss the sampling cost. We decompose $\bigotimes_{m=1}^k N_m = \bigotimes_{m=1}^k (h_{Im}I_m + h_{Xm}X_m + h_{Ym}Y_m + h_{Zm}Z_m)$, where I_m is an identity operator and X_m, Y_m and Z_m are Pauli operators which act on the m-th qubit, and $h_\alpha (\alpha \in \{I_m, X_m, Y_m, Z_m\})$ are corresponding coefficients. If we expand this term, it has exponentially increasing number of terms with k. To circumvent this problem, we consider Monte-Carlo implementation to calculate $\langle\psi^{(1)}|\bigotimes_{m=1}^k N_m|\psi^{(2)}\rangle$. From now on, for notational simplicity, we denote $\sigma_0^{(m)} = I_m$, $\sigma_1^{(m)} = X_m$, $\sigma_2^{(m)} = Y_m$, $\sigma_3^{(m)} = Z_m$, $h_0^{(m)} = h_{Im}$, $h_1^{(m)} = h_{Xm}$, $h_2^{(m)} = h_{Ym}$, and $h_3^{(m)} = h_{Zm}$. Introducing $\gamma^{(m)} = \sum_{k=0}^3 |h_k^{(m)}|$, $p_k^{(m)} = |h_k^{(m)}|/\gamma^{(m)}$, $\phi_{i_m}^{(m)} \in \mathbb{R}$, and $e^{i\phi_{i_m}^{(m)}} = h_{i_m}^{(m)}/|h_{i_m}^{(m)}|$, we have $\sum_{i_m} p_{i_m}^{(m)} = 1$ and

$$\begin{aligned} &\langle\psi^{(1)}|\bigotimes_{m=1}^k N_m|\psi^{(2)}\rangle \\ &= 2(\prod_{m=1}^k \gamma^{(m)}) \sum_{i_1,i_2,\ldots,i_k} (\prod_{m=1}^k p_{i_m}^{(m)}) \cdot \frac{1}{2} \times e^{i\sum_{m=1}^k \phi_{i_m}^{(m)}} \\ &\times \left[\mathrm{Re}(\langle\psi^{(1)}|\bigotimes_{m=1}^k \sigma_{i_m}^{(m)}|\psi^{(2)}\rangle) + i\mathrm{Im}(\langle\psi^{(1)}|\bigotimes_{m=1}^k \sigma_{i_m}^{(m)}|\psi^{(2)}\rangle)\right]. \end{aligned} \tag{A.4}$$

Therefore, we can compute $\langle\psi^{(1)}|\bigotimes_{m=1}^k N_m|\psi^{(2)}\rangle$ as follows. We generate $\bigotimes_{m=1}^k \sigma_{i_m}^{(m)}$ with probability $\prod_{m=1}^k p_{i_m}^{(m)}$ and implement a Hadamard test circuit for obtaining the real or imaginary part of $\langle\psi^{(1)}|\bigotimes_{m=1}^k N_m|\psi^{(2)}\rangle$ with probability

1/2 by changing the phase of the ancilla qubit. We define $\mu'_s = 2(\prod_{m=1}^{k}\gamma^{(m)})e^{i\sum_{m=1}^{k}\phi_{i_m}^{(m)}}b'_s$ and $\mu'_s = 2i(\prod_{m=1}^{k}\gamma^{(m)})e^{i\sum_{m=1}^{k}\phi_{i_m}^{(m)}}b'_s$ in the case of measurements of the real and imaginary part, respectively, where $b'_s \in \{-1, 1\}$ is the measurement outcomes of the ancilla qubit in the s-th measurement. Letting $\bar{x}$ denote the sample average of a random variable x, $\mathrm{E}[x]$ denote the expected value of x, and $\bar{\mu}'_s$ approximate $\langle\psi^{(1)}|\bigotimes_{m=1}^{k}N_m|\psi^{(2)}\rangle$. Denoting the number of measurements as N_{MC} and assuming $\forall m\ \gamma^{(m)} = \gamma$, we have

$$\mathrm{E}[|\bar{\mu}'_s - \langle\psi^{(1)}|\bigotimes_{m=1}^{k}N_m|\psi^{(2)}\rangle|] = O(\gamma^k/\sqrt{N_{MC}}). \tag{A.5}$$

Thus, we need

$$N_{MC} = O(\gamma^{2k}/\varepsilon^2) \tag{A.6}$$

for the required accuracy ε.

A.3 Comparison of Monte-Carlo contraction method and SVD contraction method

Here, we compare N_{MC} with N_{SVD}. Since $N_m = \sum_{i_m} h_{i_m}\sigma_{i_m}^{(m)}$, we have

$$\|N_m\|_{op} \le \sum_{i_m}|h_{i_m}|\left\|\sigma_{i_m}^{(m)}\right\|_{op} = \gamma^{(m)}, \tag{A.7}$$

where we used $\left\|\sigma_{i_m}^{(m)}\right\|_{op} = 1$.

Equations (9), (A.6) and (A.7) indicate $\gamma/\|N_{const}\|_{op} \ge 1$ and

$$\frac{N_{MC}}{N_{SVD}} = O((\gamma/\|N_{const}\|_{op})^{2k}). \tag{A.8}$$

Thus, the SVD contraction method is exponentially more efficient than the Monte-Carlo contraction method in terms of the sampling cost.

We present numerical calculations for $\gamma/\|N_{const}\|_{op}$ in order to check the superiority of the SVD contraction method over the Monte-Carlo contraction method. We obtain $10,000$ samples of N_{const} and $\|N_{const}\|_{op}$ by the procedure in Sec. 3.2 and γ from the Pauli decomposition of N_{const}. We show the average of the ratio $\gamma/\|N_{const}\|_{op}$ in Fig. A·1(a) and we found that the average value is about 1.4 for any n. Therefore, from the Eq. (A.8) and of the result in Fig. A·1(a), we can conclude that the SVD contraction method is expected to be $O((1.4)^{2k})$ times faster on average than the Monte-Carlo contraction method.

We also numerically evaluate the number of measurements for the two methods. The average of γ and

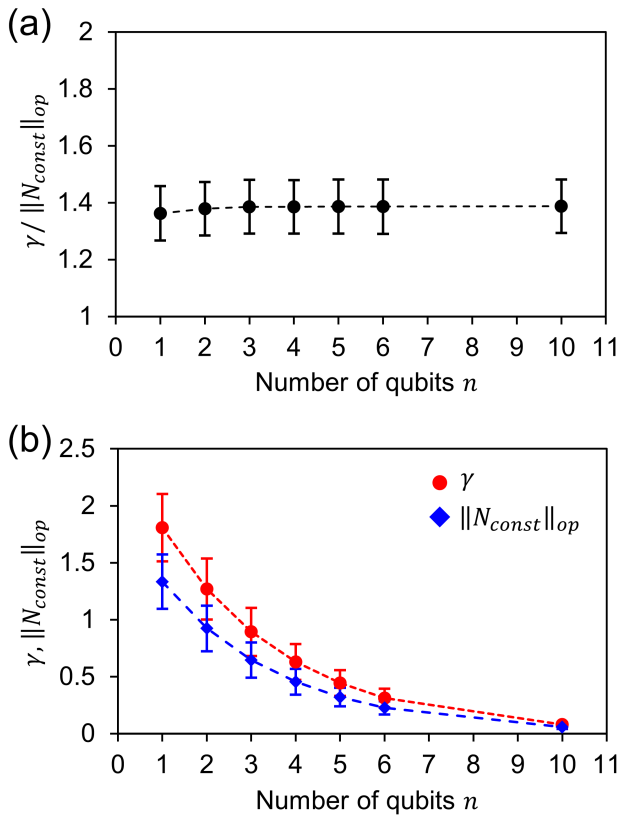

図 A·1 The average values of γ / $\|N_{const}\|_{op}$, γ, and $\|N_{const}\|_{op}$ depending on the number of qubits n (10,000 samples). Each point and error bar represents the average value and standard deviation of the samples, respectively. (a) The average value of γ / $\|N_{const}\|_{op}$. (b) The average values of γ (circle, red) and $\|N_{const}\|_{op}$ (diamond, blue).

$\|N_{const}\|_{op}$ are shown in Fig. A·1(b). In $n \ge 4$ and $n \ge 3$, γ and $\|N_{const}\|_{op}$ can be considered to be less than 1 including the standard deviation, respectively. Thus, we expect $N_{MC} \le O(1/\varepsilon^2)$ and $N_{SVD} \le O(1/\varepsilon^2)$, that is, N_{MC} and N_{SVD} are expected not to increase exponentially with k, if n is large enough.